

³¹P NMR Chemical Shift Tensors: Windows into Ruthenium Phosphinidene Complex Electronic Structures

Wesley J. Transue, Yizhe Dai, Martin-Louis Y. Riu, Gang Wu, and Christopher C. Cummins*

Cite This: *Inorg. Chem.* 2021, 60, 9254–9258

Read Online

ACCESS |

Metrics & More

Article Recommendations

Supporting Information

ABSTRACT: A series of octamethylcalix[4]pyrrole/ruthenium phosphinidene complexes ($\text{Na}_2[\mathbf{1}=\text{PR}]$) can be accessed by phosphinidene transfer from the corresponding RPA ($\mathbf{A} = \text{C}_{14}\text{H}_{10}$, anthracene) compounds ($\text{R} = \text{tBu}, \text{Pr}, \text{OEt}, \text{NH}_2, \text{NMe}_2, \text{NEt}_2, \text{N}^i\text{Pr}_2, \text{NA}, \text{dimethylpiperidino}$). Isolation of the *tert*-butyl and dimethylamino derivatives allowed comparative studies of their ^{31}P nuclear shielding tensors by magic-angle-spinning solid-state nuclear magnetic resonance spectroscopy. Density functional theory and natural chemical shielding analyses reveal the relationship between the ^{31}P chemical shift tensor and the local ruthenium/phosphorus electronic structure. The general trend observed in the ^{31}P isotropic chemical shifts for the ruthenium phosphinidene complexes was controlled by the degree of deshielding in the δ_{11} principal tensor component, which can be linked to the $\sigma_{\text{RuP}}/\pi_{\text{RuP}}^*$ energy gap. A “ $\delta_{22}-\delta_{33}$ crossover” effect for $\text{R} = \text{tBu}$ was also observed, which was caused by different degrees of deshielding associated with polarizations of the σ_{PR} and σ_{PR}^* natural bond orbitals.

Chemical shift tensors inform us about electronic structure through both their magnitudes and anisotropies, a fact readily seen through Ramsey’s classic perturbational treatment of nuclear shielding.¹ This link between the solid-state nuclear magnetic resonance (SSNMR) spectroscopy and electronic structure has proven especially useful in investigations of transition metal–ligand multiple bonds,^{2–5} including our own studies of $\text{Pn}\equiv\text{Mo}$ ($\text{Pn} = ^{15}\text{N}, ^{31}\text{P}$)^{6,7} centers. Particularly sophisticated have been the studies from the Copéret laboratory using ^{13}C magic-angle-spinning (MAS) SSNMR spectroscopy as a central tool in the design and understanding of d^0 olefin metathesis catalysts.^{8–11} While there have been studies of the ways ^{31}P chemical shifts may inform the electronic structure of transition-metal complexes,^{12,13} the field remains relatively unexplored. Against this backdrop, we have sought to expand the understanding of metal–phosphinidene bonding through ^{31}P MAS SSNMR studies.

Our recent work on phosphinidene transfer from dibenzo-7-phosphanorbornadiene RPA compounds ($\mathbf{A} = \text{C}_{14}\text{H}_{10}$ or anthracene) has positioned us well to explore [RP] unit delivery to a metal center. We now report facile phosphinidene transfer from a series of RPA compounds to the ruthenium(II) calix[4]pyrrole (“porphyrinogen”) complex $\text{Na}_2(\text{DME})_6[\mathbf{1}]$ (Figure 1, DME = 1,2-dimethoxyethane).^{14,15} The electronic structure of the resulting $\text{Ru}=\text{P}$ bond is strongly influenced by the substituent, an effect that we have characterized through ^{31}P MAS SSNMR spectroscopy. The chemical shift tensor is shown to be a direct experimental handle on the $\sigma_{\text{Ru}=\text{P}}/\pi_{\text{Ru}=\text{P}}^*$ energy gap and its orientation on the nature of the phosphorus–substituent σ_{PR} bond. Density functional theory (DFT) calculations and natural chemical shielding (NCS) analysis were central in uncovering these connections.

First investigated by Floriani et al. in 2001,^{14,15} the ruthenium(II) platform $[\mathbf{1}]^{2-}$ has been reported to support a variety of ruthenium–main group multiple bonds.^{14–16} Our

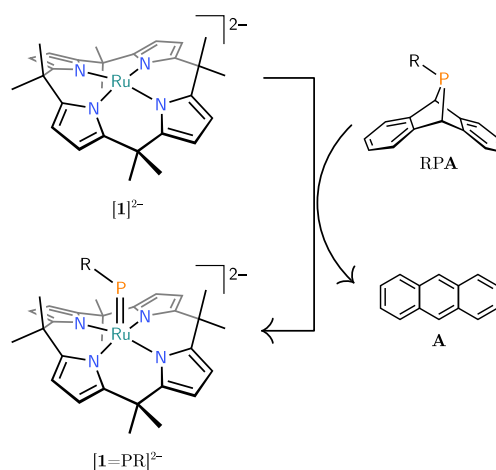
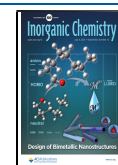


Figure 1. Ruthenium(II) complex $\text{Na}_2(\text{DME})_6[\mathbf{1}]$, which accepts phosphinidene fragments from a series of RPA compounds.

studies began by interrogating the reaction between $\text{Na}_2(\text{DME})_6[\mathbf{1}]$ and tBuPA by NMR spectroscopy in tetrahydrofuran (THF)- d_8 . Although originally reported to have a ^1H NMR spectrum consistent with $[\mathbf{1}]^{2-}$ being a closed-shell complex,¹⁷ we have found THF- d_8 solutions of $\text{Na}_2(\text{DME})_6[\mathbf{1}]$ to exhibit a single paramagnetically shifted resonance at $^1\text{H} \delta -28.3$ (s, 8H) ppm, indicating that $[\mathbf{1}]^{2-}$ is likely of intermediate spin $S = 1$, as is typical for square-planar

Received: April 12, 2021

Published: June 21, 2021



d^6 ruthenium(II) complexes.^{18–20} Monitoring the reaction between $\text{Na}_2(\text{DME})_6[\mathbf{1}]$ and ${}^t\text{BuPA}$ ²¹ over 24 h showed gradual loss of the ${}^1\text{H}$ δ -28.3 ppm resonance and growth of a new resonance in the ${}^{31}\text{P}\{^1\text{H}\}$ NMR spectrum at δ 1047 ppm, characteristic of a bent phosphinidene.²² This change was accompanied by a dramatic color change from orange-red to purple.

The reaction was relatively slow even at elevated temperatures [$k = 8.7(4) \times 10^{-4} \text{ M}^{-1} \text{ s}^{-1}$, 80 °C, THF- d_6 ; see the Supporting Information (SI), section S1.7] but could be accelerated by the addition of excess ${}^t\text{BuPA}$. Full conversion to this new species was achieved by heating $\text{Na}_2(\text{DME})_6[\mathbf{1}]$ with 3 equiv of ${}^t\text{BuPA}$ (80 °C, 18 h, THF), and the product crystallized from a hot dioxane solution to yield $\text{Na}_2(\text{dioxane})_5[\mathbf{1}=\text{P}^t\text{Bu}]$ (33% isolated) as deep-purple blocks. Characterization by an X-ray diffraction (XRD) study revealed a Ru–P–C angle of $121.57(3)^\circ$ and a Ru=P bond length of $2.1156(3)$ Å (Figure 2a), shorter than any

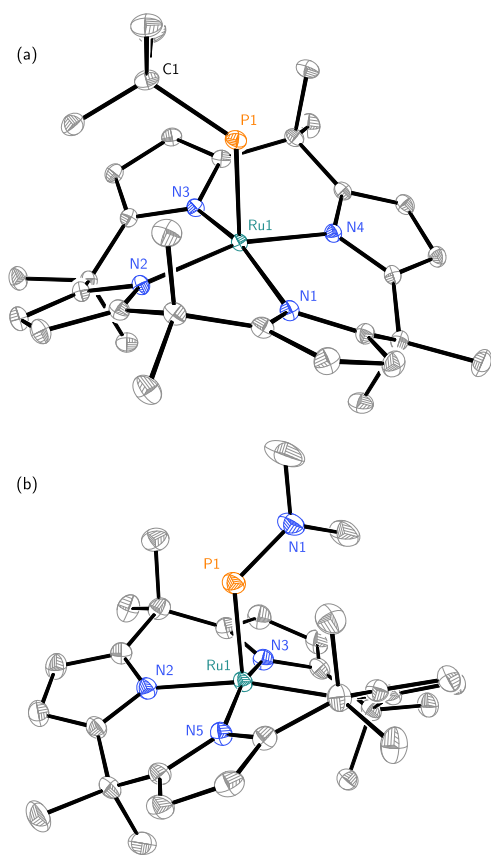


Figure 2. X-ray crystallographic structures (see the SI, section S2) of (a) $\text{Na}_2(\text{dioxane})_5[\mathbf{1}=\text{P}^t\text{Bu}]$ and (b) $\text{Na}_2(\text{dioxane})_4[\mathbf{1}=\text{PNMe}_2]$ with sodium, dioxane, and hydrogen centers omitted for clarity. (a) Selected interatomic distances (Å) and angles (deg): average Ru–N $2.0591(8)$, Ru–P $2.1156(3)$, P–C $1.8981(11)$; Ru–P–C $121.57(3)$. (b) Selected interatomic distances (Å) and angles (deg): average Ru–N $2.053(3)$, Ru–P $2.0829(8)$, P–N $1.666(3)$; Ru–P–N $121.05(11)$.

ruthenium–phosphinidene bond currently catalogued in the Cambridge Structural Database.²³ It is also slightly shorter than the sum of the two double-bond covalent radii (2.16 Å).²⁴

Similar studies combining Me_2NPA ²⁵ and $\text{Na}_2(\text{DME})_6[\mathbf{1}]$ provided analogous formation of dark purple $[\mathbf{1}=\text{PNMe}_2]^{2-}$ (18 h, 22 °C) by ${}^{31}\text{P}$ NMR spectroscopy (δ 791 ppm). The product could be isolated as a $\text{Na}_2(\text{dioxane})_4[\mathbf{1}=\text{PNMe}_2]^{2-}$ salt

following recrystallization from hot dioxane (62% isolated yield). The structural parameters from an XRD study (Figure 2b) are similar to those of $\text{Na}_2(\text{dioxane})_5[\mathbf{1}=\text{P}^t\text{Bu}]$ with a slightly shorter Ru=P bond length of $2.0829(8)$ Å and a Ru–P–N angle of $121.05(11)^\circ$.

The ruthenium calix[4]pyrrole platform proved quite versatile in phosphinidene complex formation. Treatment with a medley of RPA compounds showed successful formation of the anticipated $[\mathbf{1}=\text{PR}]^{2-}$ species in situ by ${}^{31}\text{P}$ NMR spectroscopy, resonating over a wide (~ 300 ppm) range of chemical shifts (Figure 3). The only exceptions were

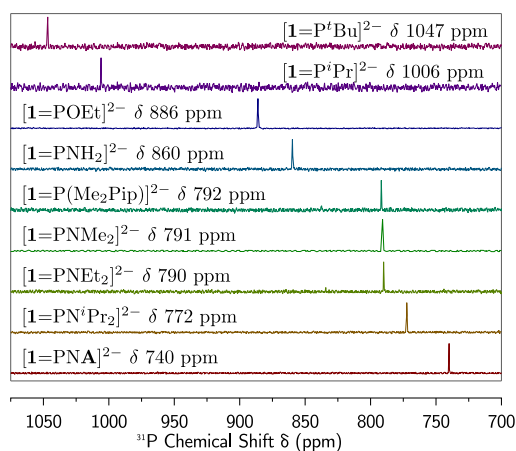


Figure 3. ${}^{31}\text{P}$ NMR spectra of several phosphinidene complexes $[\mathbf{1}=\text{PR}]^{2-}$ ($\text{Me}_2\text{Pip} = \text{cis-2,6-dimethylpiperidino}$).

CIPA ^{25,26} and HPA ,²⁷ which yielded complicated mixtures of products, and $(\text{Me}_3\text{Si})_2\text{NPA}$,²¹ which we presume was too sterically encumbered to react. Additionally, extended heating of $\text{Na}_2(\text{DME})_6[\mathbf{1}]$ with $({}^t\text{BuP})_3$ ²⁸ (48 h, 80 °C) did not lead to the observation of $[\mathbf{1}=\text{P}^t\text{Bu}]^{2-}$ in the ${}^{31}\text{P}$ NMR spectrum, indicating that RPA compounds are superior phosphinidene group transfer reagents for this transformation.

The wide range of chemical shifts demonstrated high sensitivity of the resonance to the electronic structure of the Ru=PR center. Collection of the ${}^{31}\text{P}$ MAS SSNMR spectra of $\text{Na}_2(\text{dioxane})_5[\mathbf{1}=\text{P}^t\text{Bu}]$ and $\text{Na}_2(\text{dioxane})_4[\mathbf{1}=\text{PNMe}_2]$ added insight into the nature of the phosphorus chemical shift tensors (Figure 4a,b). The large spans of the tensors ($\Omega = \delta_{11} - \delta_{33} = 1852$ and 1740 , respectively) are characteristic of multiply bonded phosphorus centers,^{7,29} and their highly negative skews [$\kappa = 3(\delta_{22} - \delta_{\text{iso}})/\Omega = -0.82$ and -0.55 , respectively] indicate a single highly deshielded direction, as expected of a double bond.^{30–33} Interestingly, the larger solution ${}^{31}\text{P}$ chemical shift δ_{sol} of $\text{Na}_2(\text{dioxane})_5[\mathbf{1}=\text{P}^t\text{Bu}]$ than that of $\text{Na}_2(\text{dioxane})_4[\mathbf{1}=\text{PNMe}_2]$ was reflected in all three directions of the chemical shift tensors obtained by simulation of the ${}^{31}\text{P}$ MAS SSNMR spectra.

Interpretation of these tensors was assisted by DFT and the NCS³⁴ analytical subroutine of the natural bond orbital (NBO) program (see the SI, section S3).³⁵ Nuclear shielding calculations yielded the tensors shown in Figure 4c–e upon variation of the substituent from *tert*-butyl to dimethylamino and methoxy. The axis of strongest deshielding (δ_{11}) uniformly resides in the Ru–P–R plane and is approximately perpendicular to the Ru–P bond, a consequence of the strong paramagnetic deshielding induced by nucleus–orbit coupling between the $\sigma_{\text{Ru}=\text{P}}$ and $\pi_{\text{Ru}=\text{P}}$ NBOs. This can be visualized

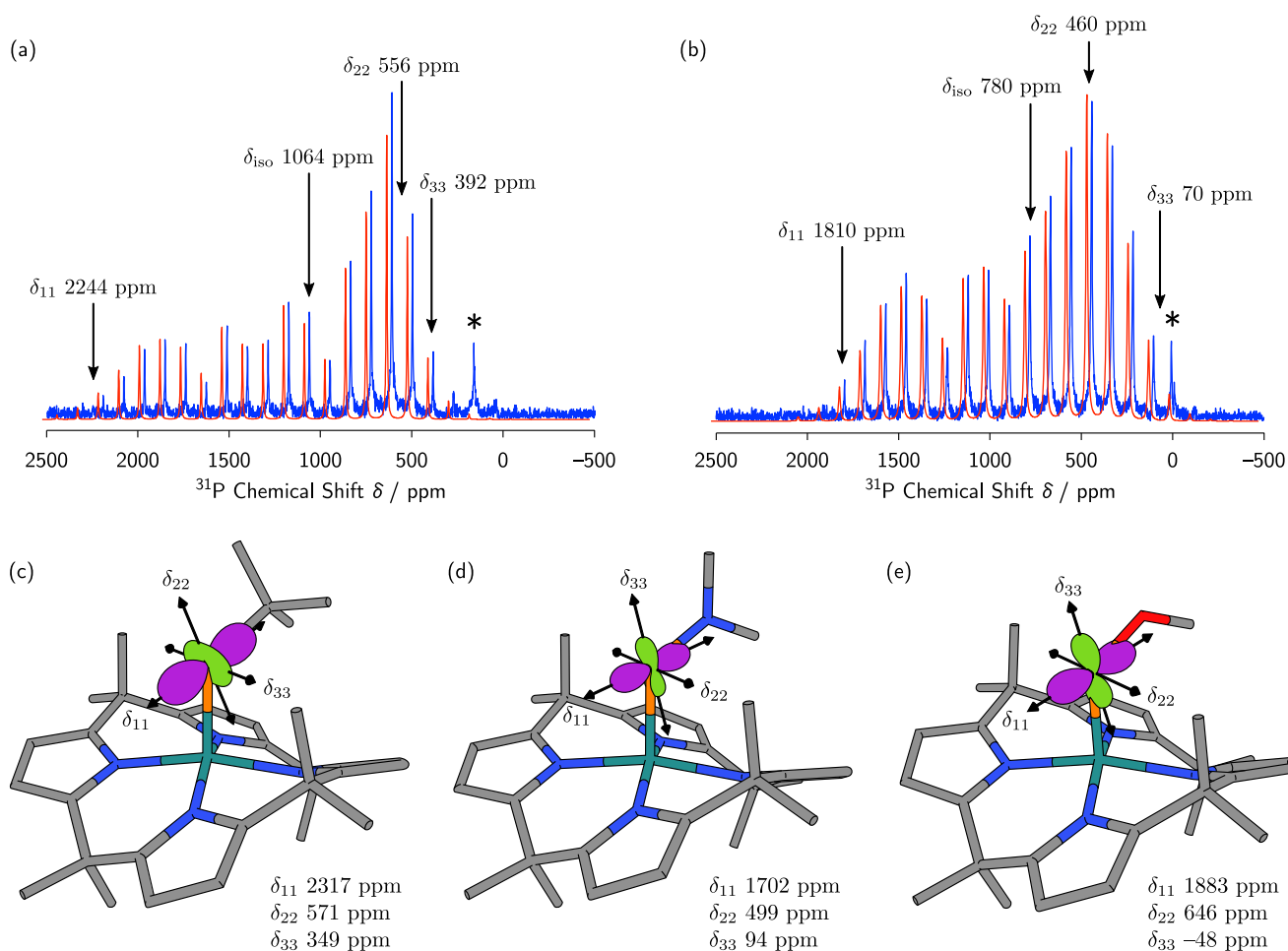


Figure 4. (a and b) Experimental (blue) and simulated (red) ^{31}P MAS SSNMR (16.4 T, 85% aqueous H_3PO_4 , δ 0 ppm) spectra of (a) $\text{Na}_2(\text{dioxane})_5[\mathbf{1}=\text{P}^t\text{Bu}]$ and (b) $\text{Na}_2(\text{dioxane})_5[\mathbf{1}=\text{PNMe}_2]$. Simulations are deliberately offset downfield for easy visual inspection. Minor impurities are marked with an asterisk (*). (c–e) Plots of the anisotropic components of the calculated chemical shift tensors for (c) $\text{Na}_2(\text{OMe}_2)_5[\mathbf{1}=\text{P}^t\text{Bu}]$, (d) $\text{Na}_2(\text{OMe}_2)_5[\mathbf{1}=\text{PNMe}_2]$, and (e) $\text{Na}_2(\text{OMe}_2)_5[\mathbf{1}=\text{POMe}]$ as $\vec{r}(\delta - \frac{1}{3}\text{Tr } \delta)\vec{r}$ for $r = (\sin \theta \cos \phi, \sin \theta \sin \phi, \cos \theta)$. Principal axes are illustrated with arrows; purple lobes indicate a downfield shift relative to δ_{iso} , and green lobes indicate upfield shift. Sodium and hydrogen atoms and molecules of solvation are omitted for clarity. Note that the directions of δ_{22}/δ_{33} are inverted in part c versus parts d and e.

as a 90° rotation of the σ bond about the δ_{11} principal axis providing significant orbital overlap with the π^* orbital. Such behavior mirrors that of the ^{13}C NMR chemical shifts for d^0 olefin metathesis catalysts.⁸ The δ_{11} contributions from the σ/π^* interaction were quantified by NCS analysis to be 1987 ppm (^tBu), 1545 ppm (NMe_2), and 1740 ppm (OMe), giving a trend that matches the solution δ_{iso} values.

Ramsey's theory of nuclear shielding can be used for a qualitative explanation of this phenomenon. Ramsey's perturbative treatment relates paramagnetic deshielding to the sum-over-states (eq 1):¹

$$\delta_{uv}^{\text{para}} \propto \sum_{k>0} \frac{\text{Re}[\langle 0|L_u|k\rangle\langle k|L_{\alpha,v}r_\alpha^{-3}|0\rangle]}{E_0 - E_k} \quad (1)$$

Here, α is the nucleus of interest (the phosphorus-31 center), u/v indexes the Cartesian directions (xyz), $|0\rangle$ is the ground state, $|k\rangle$ indexes all excited states, E_X is the energy of state X , Re indicates the real part of a complex number, L_u is the u component of the angular momentum operator, r_α is the distance from nucleus α , and $L_{\alpha,v}$ is the v component of the angular momentum operator relative to nucleus α . The low-lying $\pi_{\text{Ru}=\text{P}}^*$ orbital provides a small $E_0 - E_k$ denominator,

leading to strong deshielding.³⁶ The δ_{11} shift is thus controlled by the energy of the π^* orbital, which is, in turn, controlled by the nature of the phosphinidene substituent. Stronger donors should destabilize the $\pi_{\text{Ru}=\text{P}}^*$ orbital, so the δ_{11} shift is a direct experimental readout of the π donicity. Indeed, the *tert*-butyl derivative has the most downfield shift of the three and the strong π -donor dimethylamino derivative the most upfield shift, and the weaker π -donor methoxy derivative is intermediate.

A second interesting difference between the tensors is readily observed in Figure 4c–e, which shows that δ_{22} and δ_{33} are reversed in the *tert*-butyl derivative.^{37,38} NCS calculations clearly reveal that the orientation of the tensor is dictated by a balance of influences from the σ_{RuP} and σ_{PR} NBOs (Table S2). The σ_{PR} NBO contributes to deshielding along the Ru–P bond through coupling to the π_{RuP}^* antibonding NBO, and the σ_{RuP} NBO contributes perpendicularly to the Ru–P–R plane through coupling to the σ_{RuP}^* antibonding NBO. Both influences seem to reflect the polarization of the phosphorus–substituent interaction (Table 1). As the electronegativity of the substituent increases, the phosphorus character of the σ_{PR} NBO decreases and that of σ_{PR}^* correspondingly increases. The ^{31}P deshielding influence of the NBO parallels its

Table 1. Percent Phosphorus Character (%) of NBOs

NBO	substituent		
	^t Bu	NMe ₂	OMe
σ_{RuP}	56	47	51
σ_{RuP}^*	44	53	49
π_{RuP}	67	72	68
π_{RuP}^*	33	28	32
σ_{PR}	37	24	19
σ_{RuP}^*	63	76	81

phosphorus character, meaning the percent phosphorus character should correlate with the NBO influence. Indeed, this is seen for both the σ_{PR} contribution along the Ru–P bond (^tBu, 1166 ppm, σ_{PR} 37% P; NMe₂, 497 ppm, σ_{PR} 24% P; OMe, 405 ppm, σ_{PR} 19% P) and the σ_{RuP} contribution perpendicular to the Ru–P–R plane (^tBu, 434 ppm, σ_{PR}^* 63% P; NMe₂, 559 ppm, σ_{PR}^* 76% P; OMe, 693 ppm, σ_{PR}^* 81% P). Thus, the orientation of the δ_{22} and δ_{33} axes is an experimental reflection of the polarization of the P–R bond.

Influences on the ³¹P chemical shift tensor are undoubtedly multifaceted; however, the wide array of derivatives available from Na₂(DME)₆[1] has allowed us to map out several of the strongest factors. In this way, ³¹P MAS SSNMR spectroscopy makes experimentally accessible the local electronic structure of the Ru=PR moiety. Leverage of analogous information in d⁰ olefin metathesis catalysts has been a major influence in the design of early-transition-metal alkylidene catalysts,^{8–11} hinting that ³¹P MAS SSNMR spectroscopy may be a boon to similar advances in phosphinidene chemistry. Such analogies with metathesis and cyclopropanation catalysts were an early motive in the preparation of [I=PR]^{2–} complexes because we have recently begun to investigate catalytic “phosphirane” reactions.³⁹ We plan to use SSNMR to guide the search for further phosphinidene transfer catalysts.

■ ASSOCIATED CONTENT

SI Supporting Information

The Supporting Information is available free of charge at <https://pubs.acs.org/doi/10.1021/acs.inorgchem.1c01099>.

Full synthetic and computational details, including preparative procedures, spectroscopic data, and crystallographic data for characterization of the compounds (PDF)

Accession Codes

CCDC 2075093–2075095 contain the supplementary crystallographic data for this paper. These data can be obtained free of charge via www.ccdc.cam.ac.uk/data_request/cif, or by emailing data_request@ccdc.cam.ac.uk, or by contacting The Cambridge Crystallographic Data Centre, 12 Union Road, Cambridge CB2 1EZ, UK; fax: +44 1223 336033.

■ AUTHOR INFORMATION

Corresponding Author

Christopher C. Cummins – Department of Chemistry, Massachusetts Institute of Technology, Cambridge, Massachusetts 02139, United States; orcid.org/0000-0003-2568-3269; Email: ccummins@mit.edu

Authors

Wesley J. Transue – Department of Chemistry, Massachusetts Institute of Technology, Cambridge, Massachusetts 02139, United States; orcid.org/0000-0001-7445-5663

Yizhe Dai – Department of Chemistry, Queen's University, Kingston, Ontario K7L3N6, Canada

Martin-Louis Y. Riu – Department of Chemistry, Massachusetts Institute of Technology, Cambridge, Massachusetts 02139, United States; orcid.org/0000-0002-0900-3545

Gang Wu – Department of Chemistry, Queen's University, Kingston, Ontario K7L3N6, Canada; orcid.org/0000-0002-0936-9432

Complete contact information is available at:

<https://pubs.acs.org/10.1021/acs.inorgchem.1c01099>

Notes

The authors declare no competing financial interest.

■ ACKNOWLEDGMENTS

This material is based on research supported by the National Science Foundation under Grant CHE-1955612. G.W. thanks the NSERC of Canada for funding.

■ REFERENCES

- (1) Flygare, W. H. Magnetic interactions in molecules and an analysis of molecular electronic charge distribution from magnetic parameters. *Chem. Rev.* **1974**, *74*, 653–687.
- (2) Greco, J. B.; Peters, J. C.; Baker, T. A.; Davis, W. M.; Cummins, C. C.; Wu, G. Atomic Carbon as a Terminal Ligand: Studies of a Carbido-molybdenum Anion Featuring Solid-State ¹³C NMR Data and Proton-Transfer Self-Exchange Kinetics. *J. Am. Chem. Soc.* **2001**, *123*, 5003–5013.
- (3) Zhao, G.; Basuli, F.; Kilgore, U. J.; Fan, H.; Aneetha, H.; Huffman, J. C.; Wu, G.; Mindiola, D. J. Neutral and Zwitterionic Low-Coordinate Titanium Complexes Bearing the Terminal Phosphinidene Functionality. Structural, Spectroscopic, Theoretical, and Catalytic Studies Addressing the Ti–P Multiple Bond. *J. Am. Chem. Soc.* **2006**, *128*, 13575–13585.
- (4) Thompson, R.; Chen, C.-H.; Pink, M.; Wu, G.; Mindiola, D. J. A Nitrido Salt Reagent of Titanium. *J. Am. Chem. Soc.* **2014**, *136*, 8197–8200.
- (5) Zhu, J.; Kurahashi, T.; Fujii, H.; Wu, G. Solid-state ¹⁷O NMR and computational studies of terminal transition metal oxo compounds. *Chem. Sci.* **2012**, *3*, 391–397.
- (6) Sceats, E. L.; Figueroa, J. S.; Cummins, C. C.; Loening, N. M.; Van der Wel, P.; Griffin, R. G. Complexes obtained by electrophilic attack on a dinitrogen-derived terminal molybdenum nitride: electronic structure analysis by solid state CP/MAS ¹⁵N NMR in combination with DFT calculations. *Polyhedron* **2004**, *23*, 2751–2768.
- (7) Wu, G.; Rovnyak, D.; Johnson, M. J. A.; Zanetti, N. C.; Musaev, D. G.; Morokuma, K.; Schrock, R. R.; Griffin, R. G.; Cummins, C. C. Unusual ³¹P Chemical Shielding Tensors in Terminal Phosphido Complexes Containing a Phosphorus–Metal Triple Bond. *J. Am. Chem. Soc.* **1996**, *118*, 10654–10655.
- (8) Halbert, S.; Copéret, C.; Raynaud, C.; Eisenstein, O. Elucidating the Link between NMR Chemical Shifts and Electronic Structure in d⁰ Olefin Metathesis Catalysts. *J. Am. Chem. Soc.* **2016**, *138*, 2261–2272.
- (9) Gordon, C. P.; Yamamoto, K.; Liao, W.-C.; Allouche, F.; Andersen, R. A.; Copéret, C.; Raynaud, C.; Eisenstein, O. Metathesis Activity Encoded in the Metallacyclobutane Carbon-13 NMR Chemical Shift Tensors. *ACS Cent. Sci.* **2017**, *3*, 759–768.
- (10) Gordon, C. P.; Culver, D. B.; Conley, M. P.; Eisenstein, O.; Andersen, R. A.; Copéret, C. π -Bond Character in Metal–Alkyl

Compounds for C–H Activation: How, When, and Why? *J. Am. Chem. Soc.* **2019**, *141*, 648–656.

(11) Gordon, C. P.; Copéret, C. Metal Alkyls with Alkylidynic Metal–Carbon Bond Character: Key Electronic Structures in Alkane Metathesis Precatalysts. *Angew. Chem., Int. Ed.* **2020**, *59*, 7035–7041.

(12) Raynaud, C.; Norbert-Agaisse, E.; James, B. R.; Eisenstein, O. ³¹P Chemical Shifts in Ru(II) Phosphine Complexes. A Computational Study of the Influence of the Coordination Sphere. *Inorg. Chem.* **2020**, *59*, 17038–17048.

(13) Azofra, L. M.; Vummaleti, S. V. C.; Zhang, Z.; Poater, A.; Cavallo, L. σ/π Plasticity of NHCs on the Ruthenium–Phosphine and Ruthenium = Ylidene Bonds in Olefin Metathesis Catalysts. *Organometallics* **2020**, *39*, 3972–3982.

(14) Bonomo, L.; Stern, C.; Solari, E.; Scopelliti, R.; Floriani, C. Acetylenes Rearranging on Ruthenium–Porphyrinogen and Leading to Vinylidene and Carbene Functionalities. *Angew. Chem., Int. Ed.* **2001**, *40*, 1449–1452.

(15) Bonomo, L.; Solari, E.; Scopelliti, R.; Floriani, C. Ruthenium Nitrides: Redox Chemistry and Photolability of the Ru–Nitrido Group. *Angew. Chem., Int. Ed.* **2001**, *40*, 2529–2531.

(16) Joost, M.; Nava, M.; Transue, W. J.; Martin-Drumel, M.-A.; McCarthy, M. C.; Patterson, D.; Cummins, C. C. Sulfur monoxide thermal release from an anthracene-based precursor, spectroscopic identification, and transfer reactivity. *Proc. Natl. Acad. Sci. U. S. A.* **2018**, *115*, 5866–5871.

(17) Floriani's reported NMR experiments were conducted with a deuterated dimethyl sulfoxide solvent. We found this to result in a diamagnetic octahedral complex, which we characterized crystallographically (see the SI).

(18) Watson, L. A.; Ozerov, O. V.; Pink, M.; Caulton, K. G. Four-Coordinate, Planar Ru(II). A Triplet State as a Response to a 14-Valence Electron Configuration. *J. Am. Chem. Soc.* **2003**, *125*, 8426–8427.

(19) Askevold, B.; Khusniyarov, M. M.; Herdtweck, E.; Meyer, K.; Schneider, S. A Square-Planar Ruthenium(II) Complex with a Low-Spin Configuration. *Angew. Chem., Int. Ed.* **2010**, *49*, 7566–7569.

(20) Askevold, B.; Khusniyarov, M. M.; Kroener, W.; Gieb, K.; Müller, P.; Herdtweck, E.; Heinemann, F. W.; Diefenbach, M.; Holthausen, M. C.; Vieru, V.; Chibotaru, L. F.; Schneider, S. Square-Planar Ruthenium(II) Complexes: Control of Spin State by Pincer Ligand Functionalization. *Chem. - Eur. J.* **2015**, *21*, 579–589.

(21) Velian, A.; Cummins, C. C. Facile Synthesis of Dibenzo-7 λ^3 -phosphanorbomadiene Derivatives Using Magnesium Anthracene. *J. Am. Chem. Soc.* **2012**, *134*, 13978–13981.

(22) Cowley, A. H. Terminal Phosphinidene and Heavier Congeneric Complexes. The Quest Is Over. *Acc. Chem. Res.* **1997**, *30*, 445–451.

(23) Groom, C. R.; Bruno, I. J.; Lightfoot, M. P.; Ward, S. C. The Cambridge Structural Database. *Acta Crystallogr., Sect. B: Struct. Sci., Cryst. Eng. Mater.* **2016**, *72*, 171–179.

(24) Pyykkö, P.; Atsumi, M. Molecular Double-Bond Covalent Radii for Elements Li–E112. *Chem. - Eur. J.* **2009**, *15*, 12770–12779.

(25) Velian, A.; Nava, M.; Temprado, M.; Zhou, Y.; Field, R. W.; Cummins, C. C. A Retro Diels–Alder Route to Diphosphorus Chemistry: Molecular Precursor Synthesis, Kinetics of P₂ Transfer to 1,3-Dienes, and Detection of P₂ by Molecular Beam Mass Spectrometry. *J. Am. Chem. Soc.* **2014**, *136*, 13586–13589.

(26) Abbenseth, J.; Schneider, S. A Terminal Chlorophosphinidene Complex. *Z. Anorg. Allg. Chem.* **2020**, *646*, 565–569.

(27) Transue, W. J.; Nava, M.; Terban, M. W.; Yang, J.; Greenberg, M. W.; Wu, G.; Foreman, E. S.; Mustoe, C. L.; Kennepohl, P.; Owen, J. S.; Billinge, S. J. L.; Kulik, H. J.; Cummins, C. C. Anthracene as a Launchpad for a Phosphinidene Sulfide and for Generation of a Phosphorus–Sulfur Material Having the Composition P₂S, a Vulcanized Red Phosphorus That Is Yellow. *J. Am. Chem. Soc.* **2019**, *141*, 431–440.

(28) Wellnitz, T.; Hering-Junghans, C. Synthesis and Reactivity of Monocyclic Homoleptic Oligophosphanes. *Eur. J. Inorg. Chem.* **2021**,

2021, 8–21. Web site: <https://chemistry-europe.onlinelibrary.wiley.com/doi/pdf/10.1002/ejic.202000878>

(29) Transue, W. J.; Yang, J.; Nava, M.; Sergeyev, I. V.; Barnum, T. J.; McCarthy, M. C.; Cummins, C. C. Synthetic and Spectroscopic Investigations Enabled by Modular Synthesis of Molecular Phosphaalkyne Precursors. *J. Am. Chem. Soc.* **2018**, *140*, 17985–17991.

(30) Zilm, K. W.; Webb, G. G.; Cowley, A. H.; Pakulski, M.; Orendt, A. The nature of the phosphorus–phosphorus double bond as studied by solid-state NMR. *J. Am. Chem. Soc.* **1988**, *110*, 2032–2038.

(31) Duchamp, J. C.; Pakulski, M.; Cowley, A. H.; Zilm, K. W. Nature of the carbon–phosphorus double bond and the carbon–phosphorus triple bond as studied by solid-state NMR. *J. Am. Chem. Soc.* **1990**, *112*, 6803–6809.

(32) Gudat, D.; Hoffbauer, W.; Niecke, E.; Schoeller, W. W.; Fleischer, U.; Kutzelnigg, W. Phosphorus-31 Solid-State NMR Study of Iminophosphines: Influence of Electronic Structure and Configuration of the Double Bond on Phosphorus Shielding. *J. Am. Chem. Soc.* **1994**, *116*, 7325–7331.

(33) Geiß, D.; Arz, M. I.; Straßmann, M.; Schnakenburg, G.; Filippou, A. C. SiP Double Bonds: Experimental and Theoretical Study of an NHC-Stabilized Phosphasilylidene. *Angew. Chem.* **2015**, *127*, 2777–2782.

(34) Bohmann, J. A.; Weinhold, F.; Farrar, T. C. Natural chemical shielding analysis of nuclear magnetic resonance shielding tensors from gauge-including atomic orbital calculations. *J. Chem. Phys.* **1997**, *107*, 1173–1184.

(35) Glendening, E. D.; Badenhop, J. K.; Reed, A. E.; Carpenter, J. E.; Bohmann, J. A.; Morales, C. M.; Landis, C. R.; Weinhold, F. *NBO 6.0*; Theoretical Chemistry Institute, University of Wisconsin, Madison, WI, 2013.

(36) Pinter, B.; Smith, K. T.; Kamitani, M.; Zolnhofer, E. M.; Tran, B. L.; Fortier, S.; Pink, M.; Wu, G.; Manor, B. C.; Meyer, K.; Baik, M.-H.; Mindiola, D. J. Cyclo-P₃ Complexes of Vanadium: Redox Properties and Origin of the ³¹P NMR Chemical Shift. *J. Am. Chem. Soc.* **2015**, *137*, 15247–15261.

(37) Zhu, J.; Lau, J. Y. C.; Wu, G. A Solid-State ¹⁷O NMR Study of L-Tyrosine in Different Ionization States: Implications for Probing Tyrosine Side Chains in Proteins. *J. Phys. Chem. B* **2010**, *114*, 11681–11688.

(38) Kong, X.; Terskikh, V.; Toubaei, A.; Wu, G. A solid-state ¹⁷O NMR study of platinum-carboxylate complexes: carboplatin and oxaliplatin. *Can. J. Chem.* **2015**, *93*, 945–953.

(39) Geeson, M. B.; Transue, W. J.; Cummins, C. C. Organoiron- and Fluoride-Catalyzed Phosphinidene Transfer to Styrenic Olefins in a Stereoselective Synthesis of Unprotected Phosphiranes. *J. Am. Chem. Soc.* **2019**, *141*, 13336–13340.